RGNZ/MGPB

Rudarsko-geološko-naftni zbornik
(The Mining-Geology-Petroleum Engineering Bulletin)
DOI: 10.17794/rgn.2026.4.13

Original scientific paper

Seismic Microzonation Based on Microtremor Data for Mapping the Damage Caused by an Earthquake on Bawean Island, Gresik, East Java, Indonesia

Maulida Krisna Dewi[1], Tasya Okta Irwanda[1], Juan Pandu Gyah Nur Rochman[1]*, Amien Widodo[1], Firman Syaifuddin[1]

[1] *Department of Geophysical Engineering, Institut Teknologi Sepuluh Nopember, Surabaya, Indonesia.*

Abstract

Bawean Island in Gresik is classified as an earthquake-prone area due to fault activity in the Java Sea. An example was the earthquake of March 22nd, 2024, which damaged thousands of houses and displaced tens of thousands of residents. The focus of this research is to carry out seismic microzonation utilizing the Horizontal to Vertical Spectral Ratio method with microtremor data to identify soil characteristics and vulnerability zones in the area. The microtremor data were processed through standard HVSR procedures, including signal windowing, frequency filtering, spectral analysis, and inversion, to obtain site specific seismic parameters. The results showed that the dominant frequency (f_o) ranged from 0.65 to 4.55 Hz and H/V amplitude (A_o) from 2.01 to 6.81 to reflect variations in impedance contrast. The seismic vulnerability index (K_g) was also from 1.04 to 29.54 s/cm², while the average shear-wave velocity up to a depth of 30 meters ($\bar{V}_{S30}$) was from 112.3 to 927.28 m/s. The correlation between damage data and K_g values showed that low damage corresponded to K_g values of 0-4.8, moderate to 4.8–15, and high to >15. The four parameters, including f_o, A_o, K_g, and $\bar{V}_{S30}$ were subsequently used in Fuzzy C-Means (FCM) clustering analysis to classify the area into three vulnerability zones. A microzonation map was also generated using 148 measurement points to show the strong correlation between K_g and the observed damage levels. The results are expected to support disaster mitigation efforts and resilient spatial planning.

Keywords:
Bawean Island; Fuzzy C-Means Clustering; HVSR; Microtremor; Microzonation

1. Introduction

A shallow crustal earthquake was experienced on March 22nd, 2024 at Bawean Island in Gresik Regency, East Java. The event was triggered by the activity of an active fault with a strike-slip mechanism in the Java Sea. The epicentre of the Bawean Earthquake was identified along the Muria Fault (offshore) classified as part of the old Meratus Pattern Fault Zone and suspected to have been reactivated (**BMKG, 2024; Lunt, 2019**). According to BMKG data, the epicentre was located approximately 126 km northeast of Tuban, at a depth of 11 km, and with a magnitude of M6. An aftershock with a magnitude of M6.5 was experienced offshore 4 hours following the earthquake at approximately 114 km northeast of Tuban and a depth of 12 km (**BMKG, 2024**).

The magnitude caused extensive damage on Bawean Island, Gresik, Tuban, Surabaya, Lamongan, and Madura. The data from East Java Regional Disaster Management Agency (BPBD) showed that a total of 4,679 houses were damaged, hundreds of public facilities were affected, and approximately 33,535 residents were displaced (**CNN, 2024**). Although the moderate magnitude of the earthquake, the extent of the damage caused is an indication of the influence of local site effects, which are associated with the subsurface soil conditions. This earthquake is an indication of the existence of active tectonic structures in the Java Sea region, which is normally regarded as a region with low to moderate seismicity conditions. These conditions are an indication of the need to undertake detailed seismic microzonation in the affected areas.

An earthquake is an unpredictable natural event, and this shows the importance of developing mitigation plans based on non-destructive methods, such as microtremors (**Widodo et al., 2020**). The method uses low-frequency vibrations of the Earth for its measurement. The sources of the vibrations vary and range from natural seismic phenomena to human-induced activities (**Kanai, 1983**). An example of the most common microtremor data analysis is Horizontal to Vertical Spectral Ratio (HVSR), which compares horizontal and vertical components of ground motion to identify soil characteristics (**Nakamura, 1989; Hamimu et al., 2023**).

* Corresponding author: Juan Pandu Gyah Nur Rochman
e-mail address: juanpandu@its.ac.id

Received: 9 December 2025. Accepted: 3 April 2026.
Available online: 21 July 2026

Microtremor measurements produce an HVSR curve, which can be used to estimate subsurface characteristics, including the average shear-wave velocity of the upper 30 meters ($\overline{V}_{S30}$), which represents soil conditions in the study area. This technique also enables one to invert field observation HVSR curves to estimate depth-dependent shear-wave velocity profiles. Field HVSR curves are constructed via Fast Fourier Transform (FFT) to discern the horizontal and vertical spectra. The dominant frequency (f_0), defined as the frequency at which the H/V spectral ratio reaches its maximum, reflects the resonance frequency of the subsurface. The H/V amplitude (A_0) represents the impedance contrast between sedimentary layers and the underlying bedrock. Subsequently, the $\overline{V}_{S30}$ value, the average shear-wave velocity in the top thirty meters of the subsurface, is calculated (**Susilo et al., 2025**). The values can be used to classify soil types based on SNI 1726:2019, which serves as part of the factors in determining earthquake hazard levels (**Edison, 2022**). However, the $\overline{V}_{S30}$ inversion process requires an initial velocity model as supporting data, which is determined based on the empirical model equation proposed by **Parolai et al. (2002)**. The data used in this study were derived from both microtremor measurements and the building damage data from the Bawean Earthquake as a reference for classifying seismic vulnerability index (K_g) ranging from safe to hazardous. This correlation analysis between the actual damage conditions and microtremor parameters provides a more representative and realistic mapping of earthquake hazard potential.

BMKG data showed that aftershocks continued to occur on Bawean Island up to May 15th, 2024 with a total of 669 events recorded since the main earthquake on March 22nd, 2024. In South Egypt, while the regional seismicity is characterized as low to moderate, various studies have emphasized that local site effects play a critical role in controlling ground motion. In particular, studies that were conducted in New Luxor City revealed that areas affected by regional fault systems are likely to experience a considerable level of amplification in terms of ground motion as a result of a thick sedimentary cover, despite the absence of frequent large magnitude earthquake events (**Abdelnasser et al., 2021**). Therefore, this study used microtremor data for seismic microzonation to analyze soil characteristics in the earthquake-affected areas. This approach is consistent with previous studies that have demonstrated the widespread application of microzonation for mapping seismic conditions in various regions, including studies on liquefaction susceptibility in Mamuju and seismic vulnerability assessments in South Bengkulu (**Hadi et al., 2024; Laode et al., 2025**).

The analysis microzonation was conducted using parameters such as dominant frequency (f_0), H/V amplitude (A_0), seismic vulnerability index (K_g), and the average shear wave velocity up to a depth of 30 meters ($\overline{V}_{S30}$). Furthermore, Fuzzy C-Means (FCM) Clustering method was applied to integrate the parameters into clusters, where each data point is assigned a membership degree for each cluster in order to produce an earthquake hazard zonation map that reflected the degree of building damage (**Shihab, 2000**). This integrated approach of using the HVSR and FCM methods has been gaining popularity in various international seismic microzonation studies to enhance the objectivity of hazard classification, particularly for regions with insufficient geotechnical data. The results of this study will help support the spatial planning and disaster mitigation activities for the island of Bawean.

2. Geological and Seismological Background

Bawean Island is located in Gresik Regency, East Java Province, covers an estimated area of 200 km², and is geographically situated between 5°43'–5°52' S and 112°34'–112°44' E (**Hendratno & Khoir, 2019**). It was formed by volcanic activity in Bawean Arc which separated East Java and Pati basins. Bawean Island lies in Muria-Bawean Back-Arc Volcanism zone characterized by a NE-SW structural orientation. This pattern is also in relation to Meratus lineament and Paleogene-Neogene tectonic pathway (**Pulonggono & Martodjojo, 1994**). Moreover, the subduction of the Bawean Arc is estimated to reach a depth of 600 km and is believed to have initiated during the Pleistocene period (**Hafizh, 2022**). This subduction process triggered volcanic intrusions and formed basement rock morphologies in line with the subduction pathway. The consistency of tectonic orientations from Paleogene to Holocene also shows that the area has remained tectonically and volcanically active in its geological history (**Usman, 2012**).

The Geological Map of Bawean and Masalembo Sheets (**Aziz et al., 1993**) in **Figure 1** reflects that the stratigraphy of Bawean Island from the youngest to the oldest consists of Alluvium, Balibak Volcanic Rock Formation, Kepongan Sandstone Formation, and Gelam Limestone Formation. Alluvium (Qa) which is the youngest unit is distributed along coastal areas and is composed of cobbles, gravel, sand, and clay. The majority of the island is dominated by Balibak Volcanic Rock Formation (Qv) which is composed of lava, volcanic breccia, and tuff to form distinctive geomorphological features such as waterfalls, volcanic hills, and Lake Kastoba. Kepongan Sandstone Formation (Tmps) which consists of quartz sandstone intercalated with claystone and peat has a limited distribution. In several locations, Gelam Limestone Formation (Toml) of Tertiary age is also found to be composed of reefal, clastic, and crystalline limestones.

Bawean Island is located in the Meratus Pattern Old Fault Zone or near the Muria Fault system, considered the area suspected of experiencing fault reactivation that

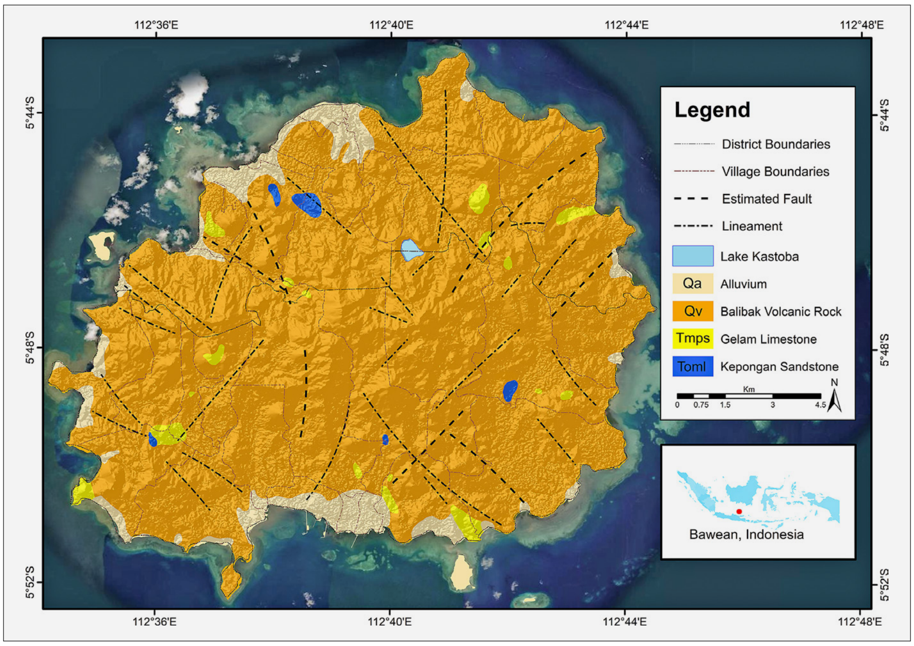

Figure 1: Regional geological map of Bawean Island dominated by the Qv Formation (Baliback Volcanic Rock) and a geological cross-section along the red line (modified from **Aziz et al., 1993**).

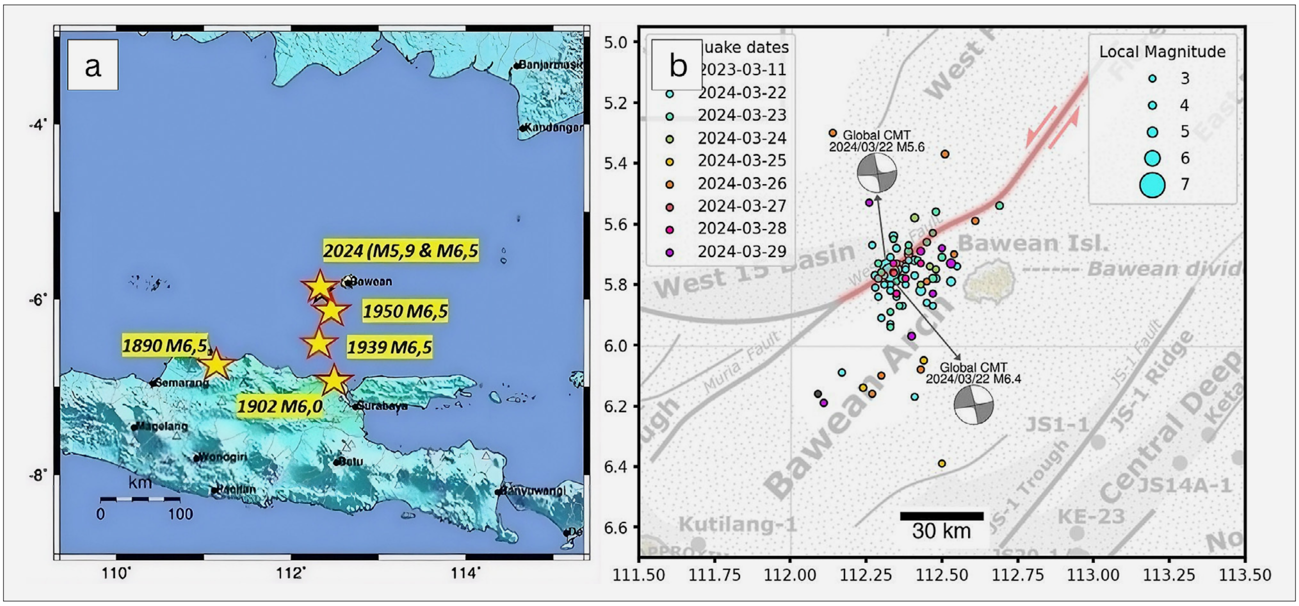

Figure 2: a) Historical earthquake data in the northern Java Sea with magnitudes ≥ M5.9 from 1890 to the present (**BMKG, 2024**) and (b) earthquake data around Bawean Island in 2024 with magnitudes ≥ M3 , plot by **Fian (2024)** using BMKG data; basemap adapted from **Lunt (2019)**.

triggered the earthquake (Lunt, 2019). The impact of this tectonic activity was the Bawean Earthquake experienced on March 22nd, 2024, at 11:22 local time (WIB). The epicentre was located offshore in 126 km northeast of Tuban, at a depth of 11 km, and with a magnitude of M6. The earthquake did not generate a tsunami, but a larger aftershock occurred at 15:53 WIB with a magnitude of M6.5, an offshore epicentre 114 km northeast of Tuban, and at a depth of 12 km.

The shaking intensity was relatively high and reached V–VI on MMI scale. This led to significant ground motion which caused the displacement of objects and low to high damage to several infrastructures. According to BMKG, it was considered one of the strongest earthquakes in the Java Sea after the Semarang 1890 earthquake (M6.5), the Gresik 1939 earthquake (M6.5), and the Gresik 1950 earthquake (M6.5), as shown in **Figure 2a**. A minimum of 669 aftershocks with magnitudes ranging from M2.1 to M6.5 have been recorded after the main event, as presented in **Figure 2b**. This large number is attributed to the heterogeneous nature of the shallow crust beneath Bawean Island, which is brittle and easily fractured. The condition contrasts with oceanic crust earthquake, where the rocks are generally more homogeneous and elastic to produce fewer aftershocks even in large-magnitude events (**Karyana, 2024**).

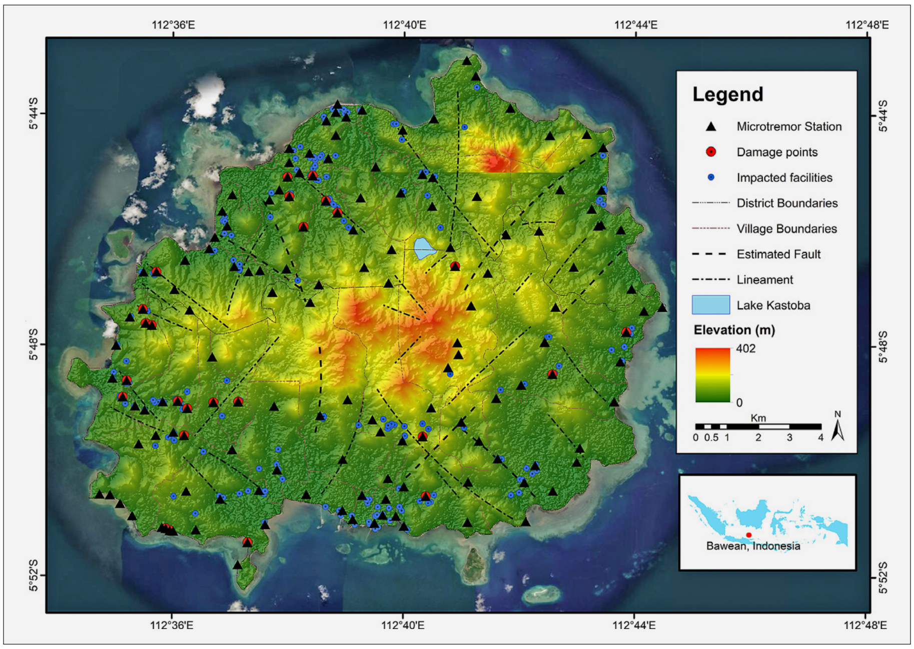

Figure 3: Microtremor stations are represented by black triangles with reference to impacted facilities in red with identified damage points caused by the 2024 Bawean Earthquake.

3. Methods

3.1. Study Area

This study used data from 148 measurement points distributed across Bawean Island in Gresik. Data acquisition was conducted from September 7th to 12th, 2024, using a Seismograf Rakyat Indonesia (SRI) system equipped with a three component sensor. During data processing, a minimum window length of 200 s was applied for spectral analysis to improve frequency resolution and spectral stability. Each measurement was recorded for approximately 20 minutes per site. The recording duration was selected to ensure sufficient data for stable H/V spectral estimation, following the recommendations of **SESAME (2004)**. The spacing along measurements varied between about 0.22 to 1.65 km adjusted according to geological conditions, building damage locations from the earthquake, site accessibility, and spatial data coverage of the entire island. The distribution of measurement points is presented in **Figure 3**. The dataset acquired consists of ambient noise recordings comprising three components including two horizontal components which are east-west and north, south as well as one vertical component in the form of up-down.

3.2. HVSR Method

The processing of the microtremor data was done by following several standard procedures of HVSR. The measurement of the microtremor was done using the Seismograf Rakyat Indonesia (SRI), which is a three-component seismograph with two horizontal components aligned in the north-south (NS) and east-west (EW) directions and the vertical component (Z). The measurement was recorded with a constant sampling rate based on the instrument specifications and an effective recording time of approximately 20 minutes. The measurements were usually performed at points at least 10 m away from residential buildings in an effort to reduce anthropogenic noise. However, in areas where buildings were damaged by the earthquake, the measurements were performed within these buildings, thus reducing the amount of human activity around the measurement points. This was mitigated by the careful selection of the data.

First, the continuous ambient noise recordings were divided into several time windows, with the minimum window length being 200 s in order to guarantee the stability of the spectral content. Windows with transient signals or heavy disturbances were eliminated by an anti-triggering method. Second, filtering was conducted to select and separate signals in the desired frequency range (**Supriyanto et al., 2023**). This process used a low-pass filter with a maximum frequency of 5 Hz and applied an anti-trigger to eliminate transient signals during acquisition. The maximum frequency of 5 Hz was selected to ensure that the analyzed frequency range remains well below the Nyquist frequency of the recorded microtremor data, thereby preventing aliasing effects. In addition, this frequency range corresponds to the dominant site frequencies associated with shallow to intermediate sedimentary layers and helps suppress high-frequency noise that is not relevant for HVSR analysis.

Third, the discrete microtremor signals in the time domain were transformed into the frequency spectrum through FFT, followed by a smoothing procedure. The signal was tapered using a cosine taper before applying spectral analysis. The spectral smoothing technique used was the Konno-Ohmachi algorithm with a constant bandwidth parameter. The smoothed spectral data of the

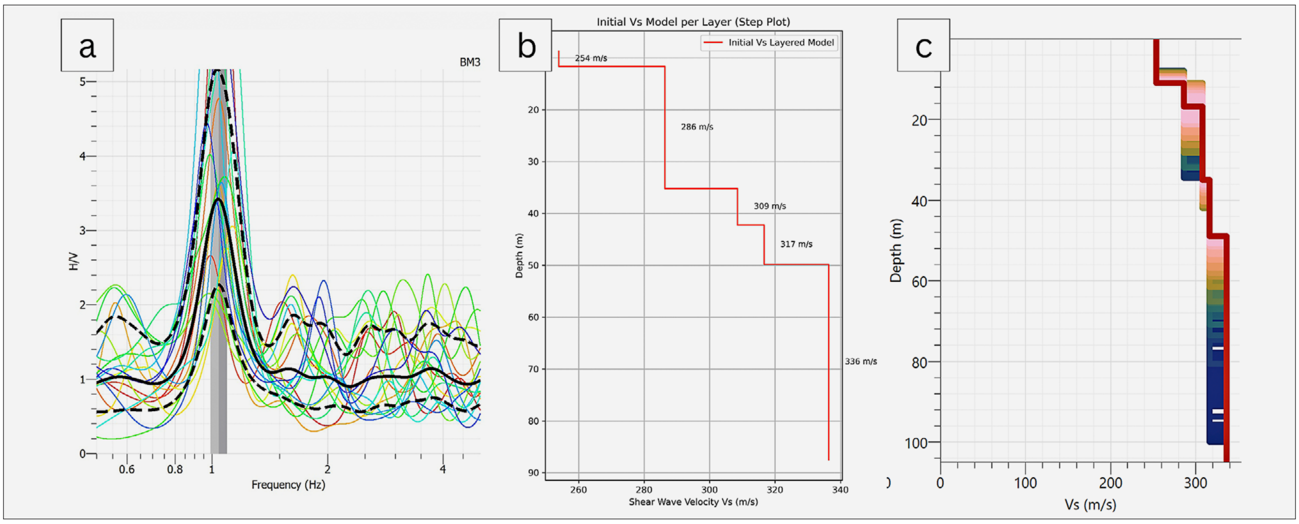

Figure 4: a) HVSR curve at BM3 obtained from Geopsy processing, (b) the initial model generated using Python, and (c) the inversion result of microtremor data showing the subsurface profile at BM3 using Dinver with the shear-wave velocity (*Vs*) distribution as a function of depth. The red line represents the best-fit inversion model while the shaded area is the model uncertainty and the boundaries of the identified subsurface layers.

horizontal and vertical components were used to obtain the HVSR curves. The average spectrum was computed for each measurement point. The dominant frequency (f_0) and H/V amplitude (A_0) were determined at the spectral peak using the average spectrum based after satisfying the reliability and clear peak criteria as shown in **Figure 4a** (**SESAME, 2004**). The reliability of the HVSR results was evaluated following the **SESAME (2004)** guidelines. The assessment included the presence of a clear and stable spectral peak, consistency of the dominant frequency across multiple time windows, and limited variability in H/V amplitude. Only curves that satisfied these reliability and clarity criteria were considered reliable and used for further analysis, while those that did not meet the criteria were excluded from subsequent interpretation.

f_0 is the most frequent value and is regarded as a characteristic of the rock layers below ground in individual sites. It allows the identification of the type and properties of the rocks. Meanwhile, A_0 is the physical contrast between the bedrock and overlying sediments due to density and seismic wave velocity contrasts, respectively (**Molnar, 2018**). f_0 and A_0 were subsequently used to calculate K_g to evaluate the degree of soil vulnerability to deformation caused by seismic shaking. The value was derived from the relationship between A_0 and f_0, as formulated by **Nakamura (2000)** and further developed by **Liu et al. (2023)** in the following equation:

$$K_g = \frac{{A_0}^2}{f_0} \quad (1)$$

Where, K_g is seismic vulnerability index, A_0 represents H/V amplitude, and f_0 is the dominant frequency.

K_g values at the damage locations were correlated with the field-based damage assessment of the Bawean Earthquake. Moreover, the damage assessment was classified according to the building damage typology developed for the 2018 Palu Earthquake by BMKG and the reference from the Ministry of Public Works and Housing (**PUPR, 2021**). The three main categories are low, moderate, and high damage. Low damage is characterized by minor wall cracks, peeling plaster, minor discolouration of building components, and low damage to ceilings or eaves without any indication of structural damage. Moderate damage refers to more serious conditions such as larger cracks, low damage to main structural elements, and damage to structural walls that are still repairable. Meanwhile, high damage is characterized by significant structural failure, such as the collapse of main walls that compromise the general stability of the building, pose safety risks to occupants, and render the building uninhabitable. The determination of the damage levels was followed by the matching of each point with the corresponding K_g at the same location. This comparison was used to evaluate the extent to which K_g could represent seismic vulnerability of the buildings.

3.3. Inversion HVSR data

The absence of ground profile or direct geotechnical information from boreholes or in-situ tests showed the need for an initial model to serve as the basis for the inversion process. The initial model was constructed by inputting an HVSR curve, applying Konno-Ohmachi smoothing, and calculating the difference to evaluate amplitude variations with depth. This curve was subsequently converted into the depth domain to allow the identification of the impedance contrasts as subsurface layer boundaries. The shear-wave velocity (*Vs*) for each layer was determined through the empirical relationship proposed by **Parolai et al. (2002)** as follows:

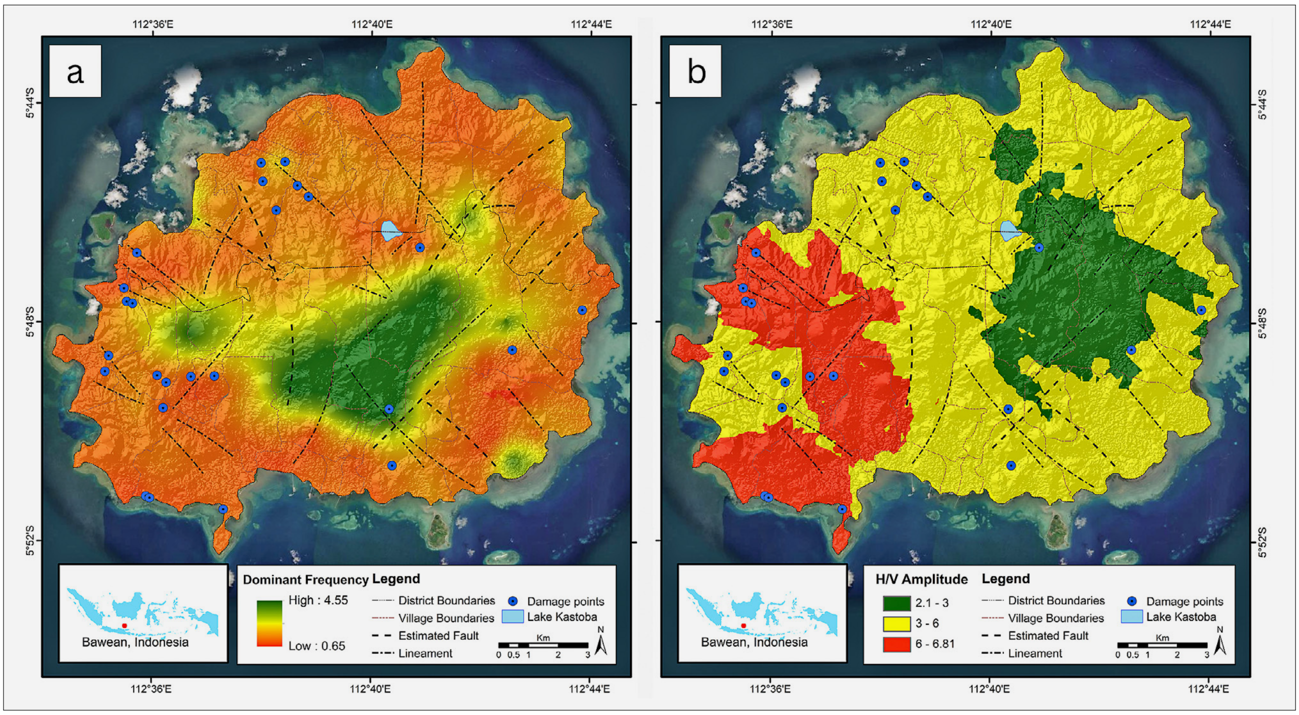

Figure 5: a) Distribution map of dominant frequency (f_o) values in Bawean Island ranging from 0.66 to 4.56 Hz, and b) distribution map of H/V amplitude (A_o) values in Bawean Island ranging from 2.1 to 6.81.

$$Vs,z = V_0\,(1+Z)^x \qquad (2)$$

Where, V_0 is the reference velocity (m/s), Z is the depth (m), and x is the empirical exponent (dimensionless) from the local USGS $\overline{V}s_{30}$ values. An example of the initial model produced is shown in **Figure 4b** which presents the identified layer boundaries and Vs profile derived from HVSR data processed.

The inversion procedure is performed by means of Dinver sub-software in the Geopsy package. The required input included HVSR curve obtained in .hv format from the previous processing stage. The others were Vs, compressional-wave velocity (Vp), Poisson's ratio (v), and density (ρ) derived from the initial model. The inputs were used to iteratively conduct the inversion using an algorithm that adjusted the subsurface model up to the period a final Vs model was obtained in line with the characteristics of HVSR data measured. The inversion results were subsequently used to calculate the average shear-wave velocity in the upper 30 meters ($\overline{V}s_{30}$) at each measurement point.

$$\overline{V}_{S30} = \frac{30}{\sum_{i=1}^{N} \frac{h_i}{v_{si}}} \qquad (3)$$

Where, h_i represents the thickness of the ith sedimentary layer (m), V_{si} is the shear-wave velocity of the ith layer (m/s), and N is the total number of layers (dimensionless). An example of the inversion result is shown in **Figure 4c** to show the subsurface profile at BM3 and depicts the distribution of Vs with depth. The estimation of Vs is important for effective earthquake disaster mitigation because the characteristics of the soil structure significantly influence risk evaluation (**Susilo et al., 2025; Syaifuddin et al. 2016**).

3.4 Fuzzy C-Means Clustering

The parameters obtained in the form of f_0, A_0, K_g, and $\overline{V}s_{30}$ were used to conduct a clustering analysis using the FCM method where each data point was assigned to clusters according to the degree of membership. The clustering process was conducted iteratively to improve classification accuracy by minimising the objective function that represented the distance between data points and the cluster centres determined based on membership values (**Shihab, 2000**). The measurements led to the identification of measurement points characterized by definite classes of seismic vulnerability, in relation to the parameter values under consideration. The information was used to delineate zones with different levels of potential earthquake-induced damage in the clustering map. The clustering was divided into three zones in this study according to the level of vulnerability to the Bawean Earthquake in line with the three categories of building damage analysis.

4. Results

4.1. Dominant Frequency (f_o)

f_0 was derived from the peak of HVSR curve on the x-axis to represent the soil response to seismic vibrations. Harder soils or bedrock generally produce a peak response at higher frequencies while softer soils or rocks tend to respond at lower frequencies. Lower f_0 values are a greater indication that sedimentary layers are thicker and Vs decreases, particularly when propagating through soft rocks (**Nakamura, 2008**). In Bawean Island, f_0 ranged from 0.65 to 4.55 Hz with higher values concentrated in the central part dominated by hilly topography while lower values were predominantly found along the coastal areas as shown in **Figure 5a**. This distribution reflects variations in subsurface sediment thickness influenced by volcanic processes, weathering, and redeposition in the Balibak Volcanic Rock Formation (Qv). An important observation is that Qv is lithologically volcanic in nature but secondary weathering has produced several zones with soft sedimentary characteristics which play a significant role in amplifying local seismic response.

The variations in f_0 values in the same geological formation show the influence of geological structures such as faults and lineaments on sediment thickness and impedance contrasts. The areas located near faults generally exhibit lower and unstable f_0 values which lead to proneness to local resonance amplifying seismic waves. This was supported by the results that most building damage points were located in areas with low f_0 values of 0.74–1.57 Hz. The trend suggested a higher seismic hazard potential in areas characterized by thick sediments and soft soils.

4.2. H/V Amplitude (A_o)

A_0 was obtained from the peak of HVSR curve on the y-axis and was used to qualitatively identify subsurface structural conditions through impedance contrast between layers (**Molnar, 2022**). **Figure 5b** shows the spatial distribution of A_0 values in Bawean Island to range from 2.01 to 6.81. The classification by **Ratdomopurbo & Suharna (2008)** shows that low amplitudes (2.01-3) are distributed in the green-shaded areas, medium (3-6) in yellow, and high (6-6.81) in red. According to **Gosar et al. (2010)** and **Molnar et al. (2022)**, A_0 reflects the impedance contrast with the bedrock but does not directly represent the actual soil amplification in a given area. The parameter is closely related to K_g because it is calculated through empirical equations with both A_0 and f_0 (**Nakamura, 1996**). Several studies also reported a correlation between H/V spectral peak and the distribution of earthquake-induced building damage (**Drajat, 2013**). Therefore, the interpretation of A_0 has certain limitations but remains relevant and practical for estimating seismic vulnerability in a particular area.

4.3. Seismic Vulnerability Index (K_g)

Microtremor data collected were supported by 25 visual documentations of building and infrastructure damage caused by the Bawean Earthquake. The documentations were used as supporting data to analyze the

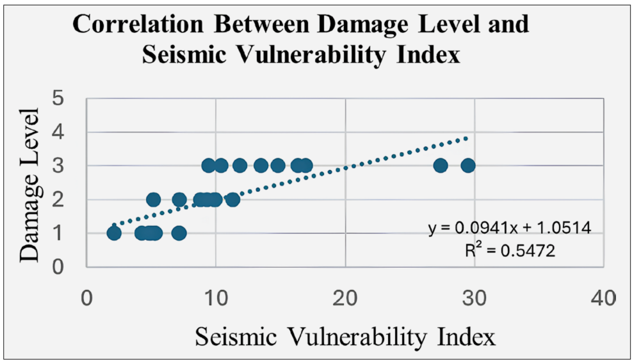

Figure 6: The relationship between seismic vulnerability index (K_g) and building damage levels based on linear regression analysis

relationship between K_g and the actual damage level observed in the field. This was achieved by classifying the damage qualitatively into three categories including low, moderate, and high. The criteria for each were based on the building damage typology from the 2018 Palu Earthquake. The damage analysis was subsequently correlated with the K_g values at the corresponding areas. The analysis was facilitated by symbolising the damage levels numerically using 1 for low, 2 for moderate, and 3 for high. A linear regression analysis was also conducted in **Figure 6** to quantify the relationship between K_g and the damage levels.

The coefficient of determination R^2 was recorded to be 0.5472 and this showed 54.72% of the variation in building damage levels could be explained by the chang-

Table 1: Classification Results for Seismic Vulnerability Index

Seismic Vulnerability Index (K_g)	Damage Category	Damage Description
0 – 4.8	Low	No structural damage was observed. The damage was only minor, affecting non-structural elements such as paint and plaster. The building remains safe and habitable.
4.8 – 15	Moderate	Cracks appeared on the walls, and structural elements were slightly affected. Components such as doors and windows experienced functional disturbances. The building is still habitable with necessary repairs.
> 15	High	Significant damage occurred to the main structural components (beams, columns, foundations). Several parts of the building are at risk of collapse. The building is unsafe for occupancy and requires evacuation and reconstruction.

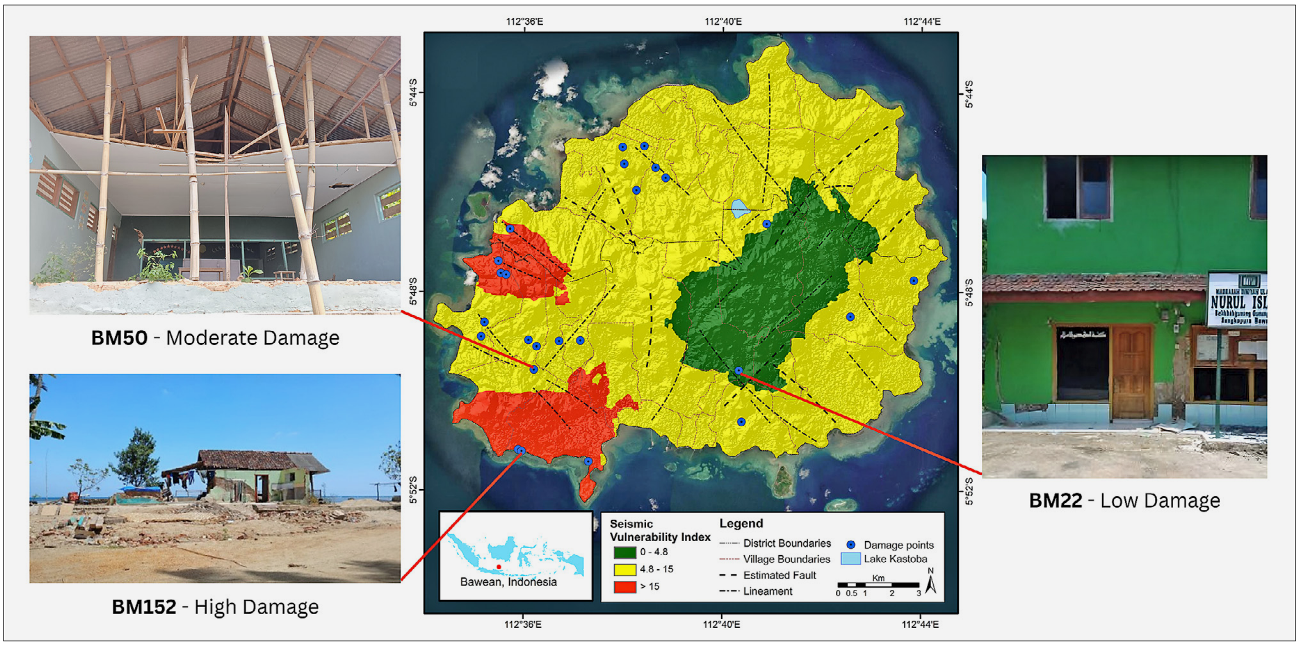

Figure 7: The distribution map of seismic vulnerability index (K_g) shows low damage at BM22 with a low-vulnerability zone (green), moderate damage at BM50 in the medium-vulnerability zone (yellow), as well as high damage and evidence of liquefaction at BM152 with the high-vulnerability zone (red).

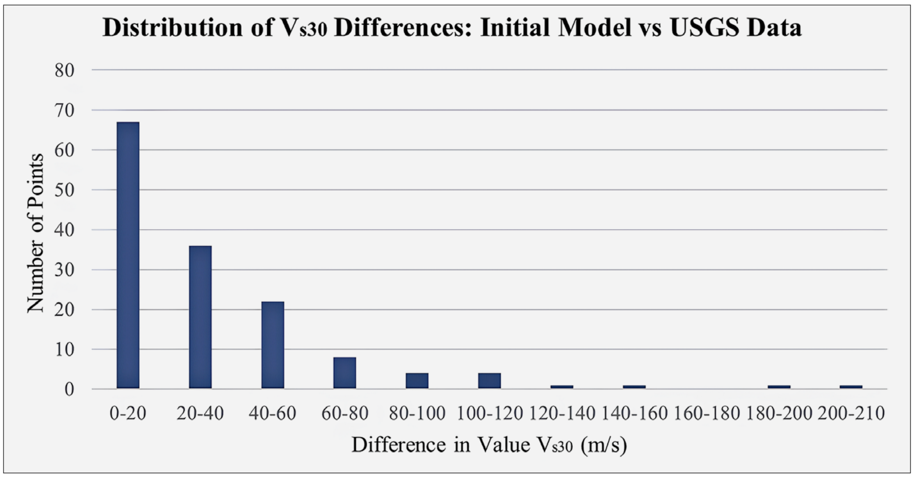

Figure 8: Histogram of the frequency distribution of the differences in $\bar{V}_{S30}$ values between the initial model and USGS data.

es in K_g. **Cohen (1998) cited in Brydges (2019)** categorized R^2 values ranging from 0.5 to 0.8 as a reflection of a reasonably good correlation. The trend showed that K_g significantly contributed to explaining the levels of building damage due to the earthquake impact in the study area. Moreover, linear regression equation y = 0.0941x + 1.0514 was used to calculate the damage classification, where x represents the K_g value for each data point. The equation determined the damage level values for each data point and the K_g threshold values corresponding to each category in **Table 1**.

The observation from the analysis is that Bawean Island has K_g values ranging from 1.04 to 29.54. **Figure 7** shows that areas with high K_g values tend to be associated with building damage caused by the Bawean Earthquake. For example, site BM152 experienced high damage that rendered the building uninhabitable and caused ground subsidence with a K_g value of 27.37. A similar condition occurred at site BM151 which exhibited high structural damage with a K_g value of 16.32. Moderate damage was observed at site BM50 with 11.31 where part of the house structure collapsed but the building remained habitable. Meanwhile, low damage such as small cracks was found at site BM22 with 4.47. The results showed that higher K_g values reflected greater potential for building damage. This trend suggested that K_g classification closely corresponded to actual damage conditions observed after the earthquake. The spatial distribution of K_g values was further used to map seismic hazard zones, as shown in **Figure 7**. The green-shaded parts represent low vulnerability typically located in stable hilly areas with minimal active geological structures. Meanwhile, red-shaded parts show high K_g values in lowland areas near the Muria Fault and lineaments

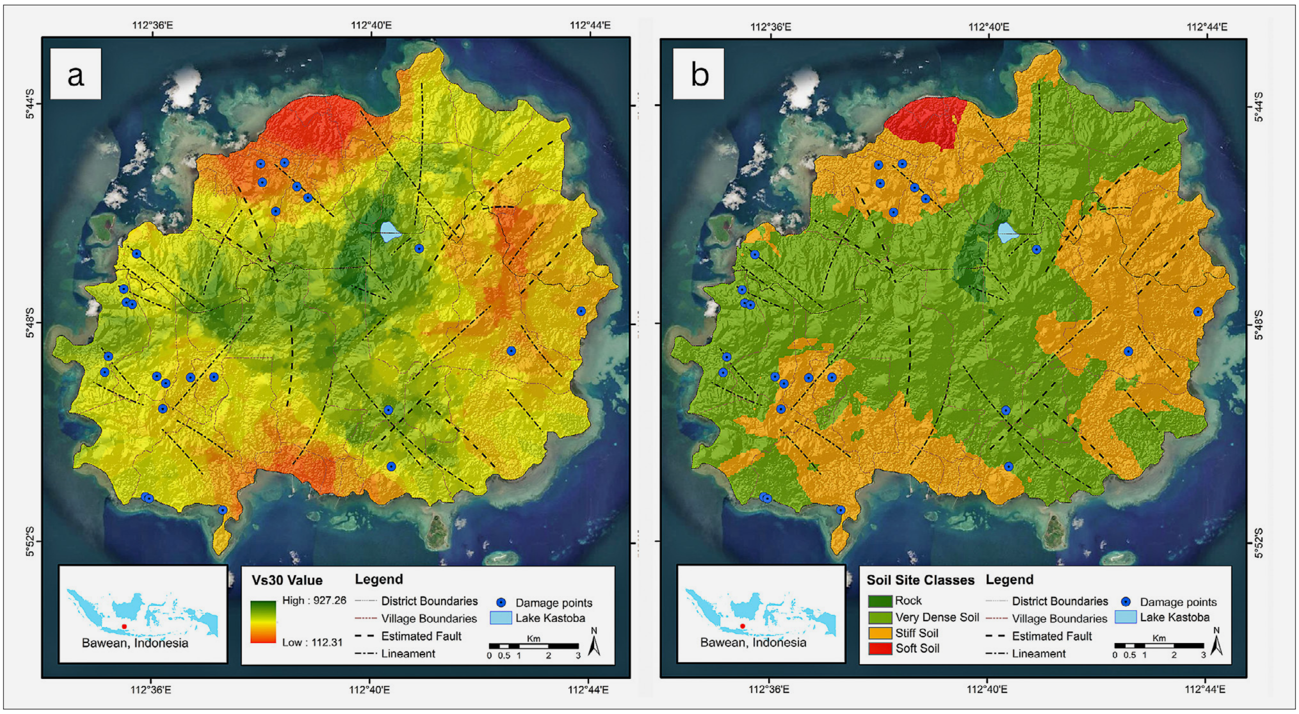

Figure 9: a) Distribution map of $\bar{V}_{S30}$ values in Bawean Island ranging from 112.31 to 927.26 m/s and b) soil site classification map based on $\bar{V}_{S30}$ values from soft soil to rock.

where heavy structural damage was recorded. The map is dominated by yellow-shaded parts representing moderately damaged areas that remain vulnerable. This was particularly focused on buildings that did not meet earthquake-resistant construction standards. The condition emphasizes that active geological structures and sediment thickness are significant in increasing K_g values and the potential for earthquake-induced damage.

4.4. Seismic Shear Velocity ($\bar{V}_{S30}$)

HVSR curves obtained in the previous step were used to construct an initial model to provide a preliminary approximation of subsurface conditions. The focus was on several soil or rock layers with each characterized by specific $\bar{V}_{S30}$, thickness, and density values.

The initial model was developed using Python software and considered valid because the differences in $\bar{V}_{S30}$ values compared to USGS data were relatively small. More than 65% were in the 0-20 m/s range and approximately 90% were below 60 m/s as shown in **Figure 8**. This reflects high consistency and accuracy which confirms the suitability of the model for further analysis and inversion.

Microtremor inversion process was used to determine the subsurface *Vs* profile using HVSR curves (*.hv) as the main input towards reflecting local resonance due to impedance contrasts. The ellipticity curve method in the Dinver module (Geopsy) was used for the inversion by matching the observed curves with theoretical models based on specific parameters. The iterations conducted up to 10,000 times produced a *Vs* profile with depth to reflect the stratigraphic conditions and physical properties of the soil. The inverted *Vs* profiles showed the velocity variations across subsurface layers and served as the basis for calculating other parameters such as $\bar{V}_{S30}$ for each site using **Equation 3**.

The modelling results of $\bar{V}_{S30}$ in the study area are visualized in **Figure 9a** with values ranging from the lowest in red to the highest in dark green. $\bar{V}_{S30}$ values varied between 112.3 m/s and 927.28 m/s with the highest concentration in the central part of the island characterized by hilly to mountainous terrain and the area surrounding Lake Kastoba. The areas are represented in dark green to reflect stiffer and more consolidated soils. The correlation with the regional geology showed that high $\bar{V}_{S30}$ values were predominantly found in areas dominated by the Balibak Volcanic Rock Formation (Qv) considered geologically denser and more stable. Meanwhile, lower values were distributed widely in coastal areas, particularly along the northern margin of the island as reflected in orange to red. This condition shows the presence of softer surface materials which tend to amplify seismic wave amplitudes. The regional geology in the areas is dominated by Alluvium deposits (Qa) which are unconsolidated and mechanically weaker.

$\bar{V}_{S30}$ in Bawean Island was further classified according to Indonesian seismic code SNI 1726 to identify soil types and stiffness characteristics in **Figure 9b**. Higher values corresponded to stiffer and more stable soils. The classification led to four soil categories with the majority of the area represented by 103 points placed into the medium soil category (SD). The stiff soil and soft rock cat-

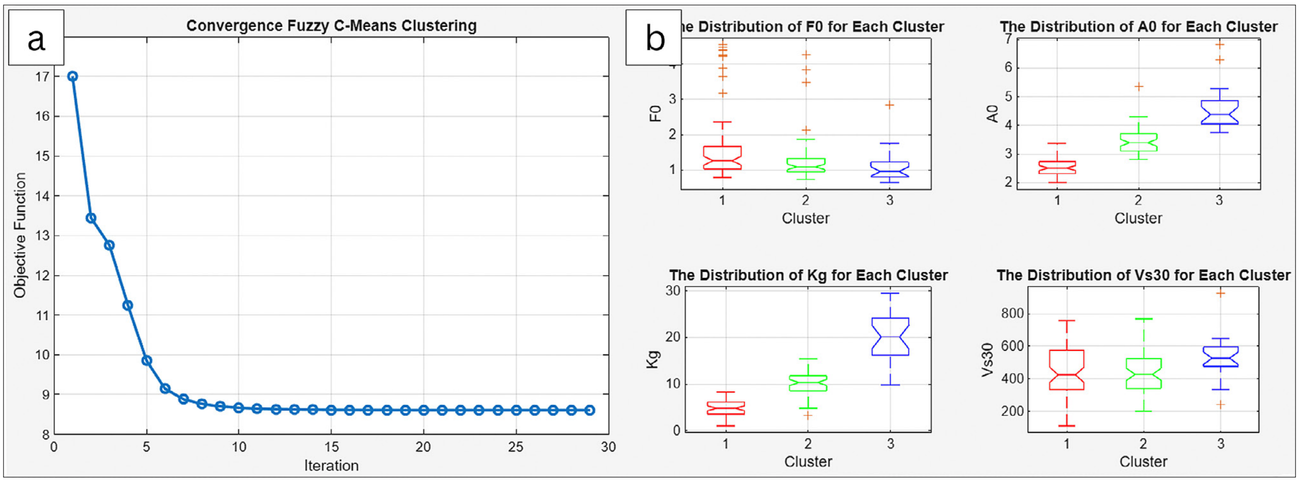

Figure 10: a) The variation of the objective function with respect to the number of iterations shows stability at the 8th iteration and b) the distribution of parameters (f_o, A_o, K_g, and $\bar{V}_{S30}$) in Cluster 1 (red), Cluster 2 (green), and Cluster 3 (blue).

egory (SC) had 40 points mostly located in areas underlain by the Balibak Volcanic Rock Formation. Meanwhile, the soft soil zone (SE) identified to have a higher potential to amplify ground shaking was mainly distributed in the northern part of the island and dominated by Alluvium deposits (Qa). The variation in $\bar{V}_{S30}$ values reflected the diverse geotechnical conditions and subsurface lithology where soft soils tended to amplify seismic shaking while stiff soils or rock layers provided better attenuation of ground motion.

5. Discussion

This study conducted clustering based on four key parameters, including f_0, A_0, K_g, and $\bar{V}_{S30}$ to map seismic hazard potential in Bawean Island. The FCM method was applied to divide the area into three hazard zones which were low, medium, and high. **Figure 10a** shows the convergence graph where the objective function reflects a significant decrease up to the 7th iteration and stabilizes after the 8th iteration. The trend is a sign that the clustering process has reached stability. Moreover, the four box plots on the right side in **Figure 10b** show the distribution of parameters in each cluster. Cluster 1 is generally characterized by relatively low f_0 and A_0 values, Cluster 2 by moderate values, and Cluster 3 by the highest values. K_g also increases progressively from Cluster 1 to 3 in line with the potential for ground amplification. However, $\bar{V}_{S30}$ exhibited a different pattern with Cluster 1 showing moderate values, Cluster 2 was lower, and Cluster 3 was higher. Although $\bar{V}_{S30}$ is used to describe the site's stiffness, the $\bar{V}_{S30}$ distribution obtained in this study may not show a monotonous relationship with the seismic hazard zones. This is an indication that the classification of the seismic hazards is influenced by the combined effect of various parameters such as the dominant frequency (f_0), H/V amplitude (A_0), and seismic vulnerability index (K_g).

Table 2: Results of FCM Clustering using f_o, A_o, K_g, and $\bar{V}_{S30}$ as input parameters.

Parameter	Cluster 1	Cluster 2	Cluster 3
f_0	1.789	1.270	1.131
A_0	2.537	3.454	4.582
K_g	4.694	10.278	20.064
$\bar{V}_{S30}$	455.588	453.728	531.504

The irregularity was because the FCM method did not depend on a single parameter but rather optimized multidimensional membership weighting across all the parameters simultaneously. The trend showed the possibility of grouping a cluster with moderate $\bar{V}_{S30}$ (Cluster 1) with low f_0 and A_0 values while a cluster with low $\bar{V}_{S30}$ (Cluster 2) was associated with moderate A_0 and K_g. This reflected that FCM did not force $\bar{V}_{S30}$ to follow a single-value pattern but rather adjusted the clustering result based on the general combination of parameters.

The clustering results led to the zonation of seismic hazard levels in the study area into three clusters. This was based on a combination of seismic hazard potential and vulnerability levels associated with seismic activity in Bawean Island. The values listed represent the average of each parameter in the respective clusters.

Table 2 confirms that the clustering using FCM divides the study area into three seismic hazard zones, including Cluster 1 for low, Cluster 2 for moderate, and Cluster 3 for high. Cluster 1 is classified as a low-hazard zone characterized by the highest f_0 of 1.789 Hz, lowest K_g of 4.694, and a maximum A_0 of 2.537. The relatively high $\bar{V}_{S30}$ of 455.588 m/s also shows that the area is dominated by relatively hard rock layers with low potential for seismic wave amplification. Cluster 2 represents a moderate-hazard zone with a f_0 of 1.270 Hz, accompanied by a significant increase in K_g at 10.278 and A_0 with 3.454. This reflects the presence of softer soil layers with a greater potential for seismic amplification compared to

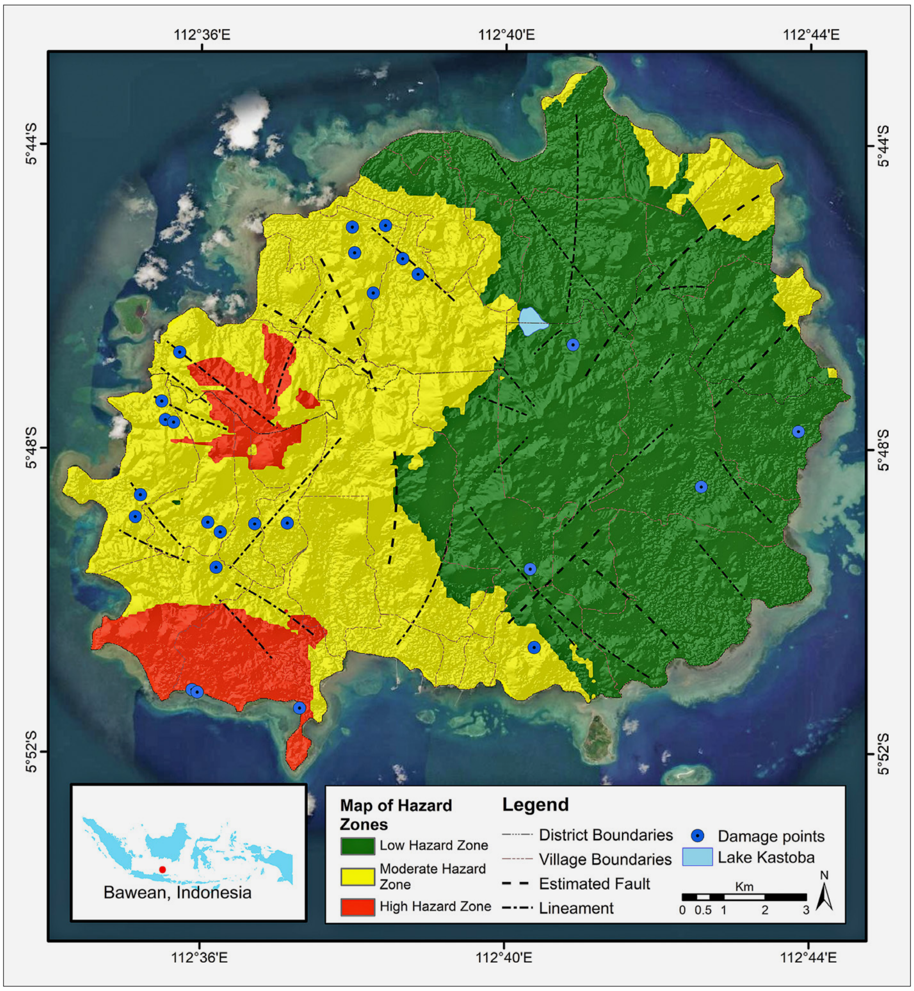

Figure 11: Seismic hazard zoning map of Bawean Island based on clustering of f_o, A_o, K_g, and $\bar{V}_{S30}$ using the FCM method

Cluster 1. The slightly lower $\bar{V}_{S30}$ value of 453.728 m/s is possibly due to thicker sediment layers which enhance the soil response to seismic waves.

Cluster 3 corresponds to the high hazard zone by showing the lowest f_0 of 1.131 Hz, the highest K_g of 20.064, and a very large A_0 of 4.582, all of which reflect very high seismic vulnerability. Interestingly, $\bar{V}_{S30}$ is 531.504 m/s which is higher than the values in Clusters 1 and 2. This elevated value is probably due to the presence of hard rock layers at greater depths in the cluster. However, the large values of A_0 and K_g categorize the area as highly vulnerable to seismic wave amplification. The non-monotonic pattern of $\bar{V}_{S30}$ between Clusters 1 and 2 is because the FCM method groups data based on the combined influence of all seismic parameters rather than a single variable. This shows that the large A_0 and K_g values justify the classification of Cluster 3 as a high hazard zone even though $\bar{V}_{S30}$ is higher.

The microzonation map in **Figure 11** shows the three seismic hazard zones which include low in green, moderate in yellow, and high in red. The low hazard zones are generally located in the eastern and central parts of the island dominated by hard rock layers, thin sediment thickness, high f_0, low A_0, low K_g, and relatively high $\bar{V}_{S30}$ values. The conditions are a reflection of a relatively low soil response to seismic shaking. The moderate hazard zones are distributed across parts of the central and northern areas of the island characterized by thicker sediment layers and intermediate seismic parameter values. In this zone, the f_0 values are generally moderate, A_0 and K_g are at intermediate levels, and $\bar{V}_{S30}$ are relatively moderate. The trend shows that the potential for seismic wave amplification exists but not at a significant level as observed in the high hazard zones.

The high hazard zones are concentrated in several areas in the western and southwestern parts of Bawean Island and represented by high K_g, large A_0, and low f_0 values. This shows the presence of thick sediment layers with a greater potential for seismic wave amplification. $\bar{V}_{S30}$ values are also generally low to reflect soft and less compact soil conditions considered more susceptible to strong ground shaking. The results were supported by field data which showed the building damage caused by the 2024 Bawean Earthquake included 60 in Lebak Village, 40 in Kumalasa Village, and 30 in Suwari Village. The spatial distribution of the hazard zones was influenced by local geological conditions including sediment thickness, rock properties, and the presence of active geological structures such as faults and lineaments. The high hazard zones are generally located near the geological structures which leads to more vulnerability to earthquake-induced ground shaking. The results of this microzonation study can serve as a scientific basis for spatial planning and disaster mitigation strategies particularly in identifying priority protection areas and planning earthquake-resilient infrastructure to minimize future seismic risks.

6. Conclusions

In conclusion, the results of analyses and mapping showed that the dominant frequency (f_0) values on Bawean Island ranged between 0.65–4.55 Hz. H/V amplitude (A_0) showed a high impedance contrast between layers at several points with values ranging from 2.01–6.81. The seismic vulnerability index (K_g) ranged from 1.04-29.54 s/cm² while the average shear-wave velocity up to a depth of 30 meters ($\bar{V}_{S30}$) was between 112.3–927.28 m/s. The correlation analysis data showed that areas with high K_g values generally experienced more high building damage. The trend reflected low damage category had K_g values ranging from 0 to 4.8, moderate from 4.8 to 15, and high was > 15. The clustering conducted using FCM produced three seismic hazard zones. These include the low zone category characterized by high f_0, low A_0, low K_g, and low $\bar{V}_{S30}$, moderate zone with intermediate parameter values, and high zone with low f_0, high A_0, high K_g, and high $\bar{V}_{S30}$. The results were supported by field data related to building damages in several villages including 60 in Lebak Village, 40 in Kumalasa Village, and 30 in Suwari Village due to the 2024 Bawean Earthquake. The produced zonation was considered accurate and could serve as an important basis for disaster mitigation, spatial planning, and infrastructure development prioritisation on Bawean Island. This study has several limitations, including the limited building damage data used for validation, the assumption of a one-dimensional subsurface structure in the HVSR method, and the estimation of $\bar{V}_{S30}$ values obtained indirectly through empirical relationships. In addition, the results of Fuzzy C-Means clustering depend on the parameters selected in the seismic hazard characterization. Therefore, further research is recommended to integrate additional geotechnical and geophysical data, such as drilled data, MASW, and combine them with maximum ground acceleration (PGA) data and earthquake scenario modelling to improve the accuracy of seismic microzonation.

Acknowledgement

The authors are grateful to the financial support provided by the Institut Teknologi Sepuluh Nopember (ITS) through the 2025 ITS Internal Research Grant Scheme under the Final Project Assistance Grant (Bantuan Tugas Akhir Mahasiswa).

7. References

Abdelnasser, M., El Khateeb, S. O., Dosoky, W., & Abbas, M. A. (2021). Site effect estimation using microtremor measurements at New Luxor City proposed site, South Egypt. Geosciences, 9(9), 008. https://doi.org/10.4236/gep.2021.99008

Aziz, S., Hardjoprawiro, S., & Mangga, S. A. (1993). Peta Geologi Lembar Bawean dan Masalembo, Jawa.

Badan Meteorologi, Klimatologi, dan Geofisika. (2024). Buletin gempabumi Stasiun Geofisika Pasuruan edisi April 2024. BMKG. https://stageof-tretes.bmkg.go.id/tulisan/20240924144735.pdf.

Brydges, R. C. (2019). Effect Size Guidelines, Sample Size Calculations, and Statistical Power in Gerontology. Innovation in Aging, Vol. 3, No. 3, 1–8.

CNN. (2024). BNPB: 4.679 Rumah Rusak Imbas Gempa Bawean, 33.533 Jiwa Mengungsi https://www.cnnindonesia.com/nasional/20240325200558-20-1078874/bnpb-4679-rumah-rusak-imbas-gempa-bawean-33533-jiwa-mengungsi diakses pada tanggal 8 November 2024 19.32

Drajat, N., Susilanto, P., Nurdiyanto, B., Pakpahan, S., & Masturyono. (2013). Efek Tapak Lokal Pada Daerah Kerusakan Akibat Gempa Bumi Bogor 9 September 2012. September 2012, 109–116.

Edison, R. (2022). Pemetaan VS30 dengan Menggunakan Korelasi Zhao di Pesisir Cilacap. Jurnal Geosaintek, 8(1), 181. https://doi.org/10.12962/j25023659.v8i1.12601

Fian, A. (2024). *Bawean EQ Swarm Epicenter (BMKG)* [Map]. Based on basemap by Lunt (2019).

Gosar, A., Rošer, J., Šket Motnikar, B., & Zupančič, P. (2010). Microtremor Study of Site Effects and Soil-Structure Resonance in The City of Ljubljana (Central Slovenia). Bulletin of earthquake engineering, 8(3), 571-592.

Hadi, A. I., Farid, M., Mase, L. Z., Refrizon, Purba, S. B., Fadli, D. I., & Sumanjaya, E. (2024). Zonation of seismic vulnerability levels in South Bengkulu Regency, Indonesia for disaster-based regional planning. Rudarsko-geološko-Naftni Zbornik, 39(2),133–148. https://doi.org/10.17794/rgn.2024.2.11

Hafizh, M. (2022). Vulkanostratigrafi Dan Petrogenesis Pulau Bawean: Studi Khusus Pada Daerah Danau Kastoba Dan Sekitarnya, Pulau Bawean, Kabupaten Gresik, Jawa Timur, Perpustakaan Digital- Digilib ITB.

Hamimu, L. H., Maindan, A., & Manan, A. (2023). Identifikasi Ketebalan Lapisan Sedimen Menggunakan Data Mikrotremor di Kecamatan Kadia Kota Kendari. Jurnal Rekayasa Geofisika Indonesia, 5(02), 98–106.

Hendratno, A., & Khoir, F. D. (2019). Petrologi Batuan Vulkanik Pulau Bawean, Kabupaten Gresik, Jawa Timur.

Kementerian Pekerjaan Umum dan Perumahan Rakyat. (2021). Laporan Pemeriksaan Cepat (Quick Assessment) Kerusakan Bangunan Gedung Pasca Bencana Gempa Bumi. Balai Pengembangan Kompetensi PUPR Wilayah IV Bandung.

Kanai, K. (1983). Engineering Seismology. In University of Tokyo Press.

Karyana, Yana. (2024). Analisis Geologi Kejadian Gempa Bumi Merusak Di Laut Jawa, Provinsi Jawa Timur, Tanggal 22 Maret 2024. https://vsi.esdm.go.id/kajian-kejadian/analisis-geologi-kejadian-gempa-bumi-merusak-di-laut-jawa-provinsi-jawa-timur-tanggal-22-maret-2024 diakses pada tanggal 8 November 19.10

Laode, A. M. W., Massinai, M. A., Ismullah Massinai, M. F., & Syamsuddin, E. (2025). Evaluating liquefaction susceptibility through HVSR and MASW methods: A case study in Mamuju, West Sulawesi, Indonesia. Rudarsko-geološko-Naftni Zbornik, 40(5), 1–18. https://doi.org/10.17794/rgn.2025.5.1

Liu, P., Wu, J., Lee, D., & Lin, Y. (2023). Detecting Landslide Vulnerability Using Anisotropic Microtremors and Vulnerability Index. Engineering Geology, 323(January), 107240.

Lunt, P. (2019). The origin of the East Java Sea Basins Deduced from Sequence Stratigraphy. Marine and Petroleum Geology, 105, 17–31. https://doi.org/10.1016/j.marpetgeo.2019.03.038

Molnar, S., Cassidy, J. F., Castellaro, S., Cornou, C., Crow, H., Hunter, J. A., Matsushima, S., Sanchez-Sesma, F. J., & Yong, A. (2018). Application of Microtremor Horizontal - to - Vertical Spectral Ratio (MHVSR) Analysis for Site Characterization : State of the Art. Surveys in Geophysics, 39(4), 613–631.

Molnar, S., Sirohey, A., Assaf, J., Bard, P. Y., Castellaro, S., Cornou, C., Cox, B., Guillier, B., Hassani, B., Kawase, H., Matsushima, S., Sánchez-Sesma, F. J., & Yong, A. (2022). A Review of the Microtremor Horizontal-to-Vertical Spectral Ratio (MHVSR) Method. In Journal of Seismology (Vol. 26, Issue 4). Springer Netherlands.

Nakamura, Y. (1989). A Method for Dynamic Characteristics Estimation of Subsurface using Microtremor on the Ground Surface. In Quarterly Reports, Railway Technical Research Institute (Vol. 30, pp. 25–33).

Nakamura, Y. (1996). Real Time Information Systems for Hazards Mitigation. Eleventh Wordl Conference on Earthquake Engineering.

Nakamura, Y. (2000). Clear Identification of Fundamental Idea of Nakamura' s Technique and its Applications. The 12th World Conference on Earthquake Engineering, Auckland, New Zealand, 30 January-4 February 2000.

Nakamura, Y. (2008). On The H/V Spectrum. the 14th world conference on eathquake engineering , 1-10.

Parolai, S., Bormann, P., & Milkereit, C. (2002). New Relationships between Vs, Thickness of Sediments, and Resonance Frequency Calculated by the H/V Ratio of Seismic Noise for the Cologne Area (Germany). Bulletin of the Seismological Society of America, 92(6), 2521–2527. https://doi.org/10.1785/0120010248

Pulonggono, A. D., and S. Martodjojo (1994). Perubahan tektonik Paleogen Neogen merupakan peristiwa tektonik terpenting di Jawa, in Geologi dan Geotek Pulau Jawa, Yogyakarta, pp. 37–39.

Ratdomopurbo, A. & Suharna (2008). Pedoman Pemetaan Mikrozonasi, Badan Geologi, Departemen Energi dan Sumberdaya Mineral, Bandung.

SESAME. (2004). Guidelines for The Implementation of the H/V Spectral Ratio Technique on Ambient Vibrations Measurements, Processing and Interpretation. Bulletin of Earthquake Engineering.

Shihab, A. I. (2000). Fuzzy Clustering Agorithms And Their Application To Medical Image Analysis. University of London, June, 406–415.

Susilo, A., Zulaikah, S., Fauzi, A., Ilham, I., Ma'muri, M., Wirawan, K., Haniyyah, S., Zarkoni, A., Persada, Y. D., Bery, A. A., & Hasan, M. F. R. (2025). Seismic site characterization of Malang Regency (Indonesia) using HVSR inversion. Kuwait Journal of Science, 53(1), 100486. https://doi.org/10.1016/j.kjs.2025.100486

Supriyanto, E., Fitriyanto A., Nurfaizah Y. (2023). Rancang Bangun Modul Low Pass Filter (LPF) Orde 1 dan Orde 2 Sebagai Penunjang Praktikum Rangkaian Elektronika dan Bengkel Elektronika Komunikasi. Integrated Lab Journal, 11 (2), 22-33.

Syaifuddin F., Bahri A. S., Lestari W. and Pandu J. (2016). Microtremor study of Gunung Anyar mud volcano, Surabaya, East Java AIP Conf. Proc. 1730 050004

Usman, E., (2012). Tektonik dan Jalur Vulkanik Busur Belakang BaweanMuria sebagai Pengontrol Pembentukan Cekungan Pati dan Potensi Hidorkarbon: Indonesian Journal of Applied Sciences (IJAS), vol.2, No.3

Widodo, A., Rochman, J. P. G. N., Perdana, A., & Syaifuddin, F. (2020). Seismic Site Effect Mapping Based on Natural Frequency Using Microtremor Method in Sidoarjo District. IOP Conference Series: Earth and Environmental Science, 506(1), 012053. https://doi.org/10.1088/1755-1315/506/1/012053.

SAŽETAK

Seizmičko mikrozoniranje temeljeno na mikrotremorskim podatcima za kartiranje oštećenja uzrokovanih potresom na otoku Bawean (Gresik, Istočna Java, Indonezija)

Otok Bawean u području Gresika svrstava se u područje s visokim seizmičkim rizikom zbog aktivnosti rasjeda u Javanskome moru. Potres koji se dogodio 22. ožujka 2024. godine uzrokovao je oštećenje tisuća kuća i raseljavanje desetaka tisuća stanovnika. Cilj je ovoga istraživanja provedba seizmičkoga mikrozoniranja primjenom metode HVSR na temelju podataka mikrotremora kako bi se identificirala svojstva tla i zone ranjivosti. Podatci mikrotremora obrađeni su standardnim HVSR postupcima, uključujući segmentiranje signala, frekvencijsko filtriranje, spektralnu analizu i inverziju, kako bi se dobili lokacijski specifični seizmički parametri. Rezultati pokazuju da se dominantna frekvencija (f_0) kreće u rasponu od 0,65 do 4,55 Hz, dok se amplitudni omjer H/V (A_0) kreće između 2,01 i 6,81, što odražava varijacije u kontrastu impedancije. Indeks seizmičke ranjivosti (K_g) kreće se od 1,04 do 29,54 s/cm², dok je prosječna brzina posmičnih valova do dubine od 30 metara ($\bar{V}_{S30}$) u rasponu od 112,3 do 927,28 m/s. Korelacija između podataka o oštećenjima i vrijednosti K_g pokazuje da niska razina oštećenja odgovara rasponu 0 – 4,8, umjerena 4,8 – 15, a visoka vrijednostima većim od 15. Nadalje, uz primjenu metode grupiranja Fuzzy C-Means (FCM) i četiriju parametara (f_0, A_0, K_g i $\bar{V}_{S30}$) područje je klasificirano u tri zone seizmičke ranjivosti. Na temelju 148 mjernih točaka izrađena je karta mikrozoniranja koja pokazuje snažnu povezanost između indeksa seizmičke ranjivosti i opaženih razina oštećenja. Dobiveni rezultati mogu doprinijeti ublažavanju posljedica potresa i otpornijem prostornom planiranju.

Ključne riječi:
Fuzzy C-Means klasterizacija, HVSR, mikrotremor, mikrozoniranje, seizmička ranjivost

Author’s contribution

Maulida Krisna Dewi contributed to field investigation, data processing, visualization, writing-original manuscript, writing-review, and editing. **Tasya Okta Irwanda** contributed to field investigation, data processing, and writing-original manuscript. **Juan Pandu Gyah Nur Rochman** contributed to review and editing, academic supervision, and overall guidance of the research. **Amien Widodo** and **Firman Syaifuddin** contributed to conceptual supervision and methodological guidance of the research.
All authors have read and agreed to the published version of the manuscript.